

Spin reorientation transition of ferromagnetic nanowires with perpendicular magnetic anisotropy

Sug-Bong Choe^{a)}*Department of Physics, Seoul National University, Seoul 151-742, Republic of Korea*

(Received 19 November 2007; accepted 24 January 2008; published online 14 February 2008)

We present an analytic theory of the magnetization phase in ferromagnetic nanowires with perpendicular magnetic anisotropy. In nanowire geometry, the shape anisotropy is reduced considerably in contrast to continuous films. Consequently, the spin reorientation transition occurs from in plane to out of plane with respect to the wire width. The stable domain size in the out-of-plane phase is sensitive to the wire width and approaches the single domain state on narrowing the width further. A phase diagram of the three phases is proposed with respect to the wire width and the saturation magnetization. © 2008 American Institute of Physics.

[DOI: 10.1063/1.2857542]

In recent years, ferromagnetic nanowires have drawn great attention due to their potential applications in memory and logic devices.^{1,2} The early studies mainly examined Permalloy nanowires with in-plane magnetic anisotropy.¹⁻⁸ Despite their successful proofs of the principles, the complex domain-wall structures and their chaotic evolution impeded technological accessibility.⁶⁻⁸ For better stability and reliability with smaller domain structures, nanowires with perpendicular magnetic anisotropy have recently been proposed and studied extensively. Perpendicularly magnetized films have three distinct domain structures: large (or single), stripe, and scattered-dot domains.⁹⁻¹¹ The large-domain phase, which shows the wall-motion-dominated reversal process, might be suitable for domain-wall-based nanowire applications. In contrast, the narrow stripe or dot domain phase gains stability in randomly written domain bits. Therefore, optimizing the stable domain phase in nanowires is crucial. In this letter, we report the stability of the magnetic domains in ferromagnetic nanowires with perpendicular magnetic anisotropy.

For this study, we modeled an infinitely long nanowire structure lying along the x axis with width w and thickness t . The direction of magnetization was assumed to vary along the x axis only. Periodic stripe domains with alternating $\pm z$ magnetization were placed with period d . Bloch walls rather than the Néel walls were considered due to their lower magnetostatic energy in this geometry. Inside the Bloch walls, the magnetization rotated in the YZ plane and the wall configuration was assumed to be $\cos \theta = \tanh[\alpha(x-x_0)/l]$,¹² where x_0 is the center of the domain wall and θ is the angle of the magnetization vector from the z axis. The wall width l was defined as the width of the area of $|m_y| \geq |m_z|$ with the choice of $\alpha = 2 \tanh^{-1}(\sqrt{\frac{1}{2}})$. The polarity of the wall was set antiparallel to the neighboring walls to lower the dipolar coupling energy. The magnetization was then transformed into a Fourier series as

$$m_z = \cos \theta(x) = \sum_{k=-\infty}^{\infty} C_k e^{i2\pi kx/d}$$

$$m_y = \sin \theta(x) = \sum_{k=-\infty}^{\infty} S_k e^{i2\pi kx/d}. \quad (1)$$

The Fourier coefficients C_k and S_k were evaluated by numerical integration using a fast Fourier transformation algorithm. Locating the origin at the center of a domain, the symmetry resulted in the condition that C_k was a real number with $C_k = C_{-k}$ and S_k was a pure imaginary number with $S_k = -S_{-k}$.

The magnetic energies were then calculated explicitly with the Fourier coefficients, including the anisotropy, exchange, and magnetostatic energies.¹³ The uniaxial magnetic anisotropy K_U , which was composed of magnetocrystalline and interface anisotropy, was set perpendicular to the film plane, i.e., along the z axis. The anisotropy energy density γ_A was then given by

$$\gamma_A = K_U \left[1 - \frac{1}{d} \int_{-d/2}^{d/2} \cos^2 \theta(x) dx \right] = K_U \left(1 - \sum_{k=-\infty}^{\infty} |C_k|^2 \right). \quad (2)$$

The exchange energy density γ_X can be written as

$$\gamma_X = \frac{A_X}{d} \int_{-d/2}^{d/2} \left(\frac{\partial \theta}{\partial x} \right)^2 dx = A_X \sum_{k=-\infty}^{\infty} \left(\frac{2\pi k}{d} \right)^2 (|C_k|^2 + |S_k|^2), \quad (3)$$

where A_X is the exchange stiffness constant.

The magnetostatic energy was calculated based on the surface magnetization density at the four surfaces of the nanowire. The magnetostatic potential from the surface magnetization density was then obtained by integration over the surfaces. Finally, the magnetostatic energy density was given by

$$\gamma_D = \frac{\mu_0 M_S^2}{2} \sum_{k=1}^{\infty} [|C_k|^2 F_k^{(w,t)} + |S_k|^2 F_k^{(t,w)}], \quad (4)$$

where

$$F_k^{(w,t)} = \int_0^{\infty} f^{(w,t)}(s) \cos\left(\frac{2\pi ks}{d}\right) ds,$$

with

^{a)}Electronic mail: sugbong@snu.ac.kr.

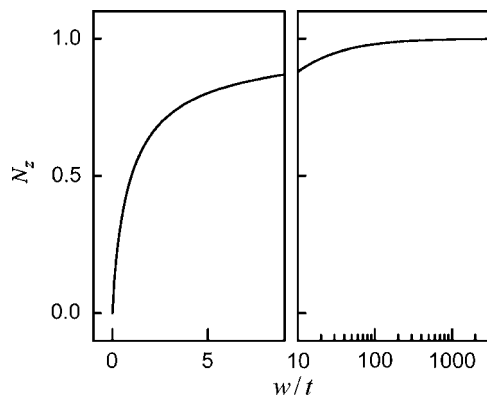


FIG. 1. The demagnetizing factor N_z with respect to the aspect ratio w/t .

$$f^{(w,t)}(s) = \frac{4}{\pi w t} \left[\sqrt{s^2 + w^2 + t^2} - \sqrt{s^2 + w^2} - \sqrt{s^2 + t^2} + \sqrt{s^2} \right. \\ \left. + w \ln \left(\frac{\sqrt{s^2 + w^2} + w}{\sqrt{s^2 + w^2 + t^2} + w} \frac{\sqrt{s^2 + t^2}}{\sqrt{s^2}} \right) \right].$$

As $s \rightarrow \infty$, $f^{(w,t)}(s) \rightarrow wt / \pi s^3$ and the numerical integration of $F_k^{(w,t)}$ was achieved quickly with good precision.

As a special case, the demagnetizing factor of the nanowires could be derived analytically. The demagnetizing factor N_z along the z axis was given by

$$N_z = F_0^{(w,t)} = \frac{2}{\pi} \tan^{-1} \left(\frac{w}{t} \right) - \frac{t}{2\pi w} \log \left[1 + \left(\frac{w}{t} \right)^2 \right] \\ + \frac{w}{2\pi t} \log \left[1 + \left(\frac{t}{w} \right)^2 \right].$$

The other components were $N_y = 1 - N_z$ and $N_x = 0$. Figure 1 plots N_z against the aspect ratio w/t . Expecting the demagnetizing factor to decrease with the aspect ratio is quite natural due to the restriction of the dipolar coupling within the narrow nanowire structure. However, we emphasize that it can cause a spin reorientation transition in nanowires. Note that the effective magnetic anisotropy K_{eff} is given by $K_{\text{eff}} = K_U - N_z(\mu_0 M_S^2 / 2)$. A negative K_{eff} prefers in-plane magnetization and a positive K_{eff} prefers out-of-plane magnetization. The spin reorientation transition basically occurs when K_{eff} changes sign. From the width-dependent N_z , this is possible by changing the nanowire width in a film.

To examine the detailed variation in the magnetization state, we evaluated the domain structure parameters l_0 and d_0 of the ground energy state by minimizing the total energy $\gamma_T(l, d)$, defined as $\gamma_T = \gamma_A + \gamma_X + \gamma_D$ with respect to l and d . Figure 2(a) shows the estimated ground energy $\gamma_T(l_0, d_0)$ with respect to the wire width w for 20-nm-thick nanowires with $K_U = 5 \times 10^5 \text{ J/m}^3$ and $A_X = 1 \times 10^{-11} \text{ J/m}$. Here, the saturation magnetization M_S was set as $1.25 M_0$, where $\frac{1}{2} \mu_0 M_0^2 = K_U$. Note that continuous thin films with these magnetic properties have strong in-plane magnetic anisotropy. In the figure, the solid line shows the ground energy of the stripe domain phase with respect to the wire width. For comparison, the dashed line indicates the energy density γ_{\perp} for the case of a single domain magnetized perpendicular to the plane and the dotted line denotes the energy density γ_{\parallel} for the case of a single domain magnetized in the plane along the x axis. The figure clearly shows that a spin reorientation transition occurred with respect to the wire width: narrow wires preferred the single domain phase magnetized perpendicularly, whereas wide wires preferred the in-plane magnetization phase. The stripe domains appeared between the two phases. The domain period d_0 and the domain wall width l_0 in the stripe domain phase are illustrated in Fig. 2(b). The domain period increased as the wires narrowed and, finally, the single domain transition occurred when the domain size exceeded the finite size of the magnetic structure.¹⁴

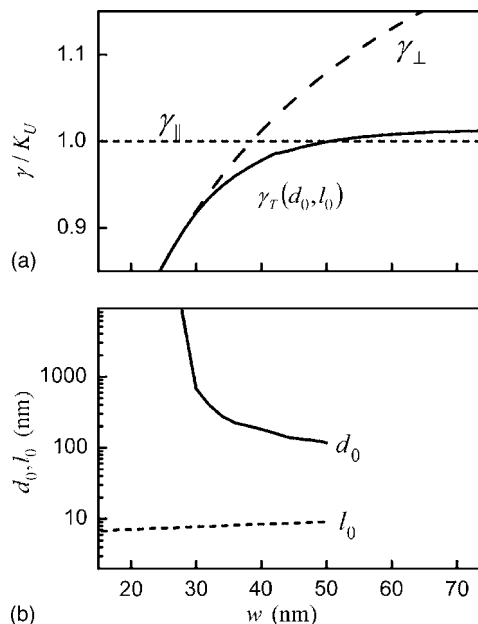


FIG. 2. (a) The solid line illustrates the ground energy with respect to the wire width for $M_S = 1.25 M_0$. The dashed and dotted lines show the values for the out-of-plane and in-plane single domain phases, respectively. (b) The stable domain period (solid line) and the domain wall width (dashed line) with respect to the wire width.

Based on these observations, we calculated the phase diagram illustrated in Fig. 3. The abscissa is the wire width on a logarithmic scale and the ordinate is the saturation magnetization normalized by M_0 . The gray contrast corresponds to the estimated domain period as designated by the color bar. The in-plane phase for $\gamma_{\parallel} < \gamma_T(l_0, d_0)$ is filled with white. Three distinct phases are clearly seen in the figure: the in-plane magnetization phase (white region), stripe domain phase (gray region), and single domain phase (black region). The solid lines are visual guides to the phase boundaries. The phase boundary line between the single domain and stripe domain phases was determined by the condition $d_0 = 10 \mu\text{m}$

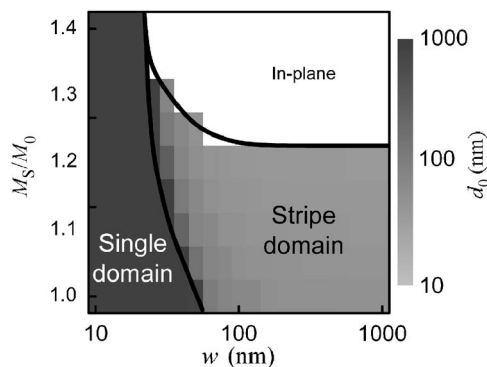


FIG. 3. The phase diagram with respect to the wire width and saturation magnetization. The gray contrast corresponds to the stable domain period as designated to the right. Three distinct phases are seen inside the figure.

as the limit of the practical magnetic device size.

Note that stable domains smaller than 100 nm could be realized. Such small domains gain information storage density in technological applications. These domains appeared adjacent to the spin reorientation transition. The smallest domains on 100-nm-wide wires were estimated to be about 40 nm in size. Conversely, large (or single) domains appeared in wires a few tens of nanometers wide.

This study was supported by the Korea Science and Engineering Foundation through the NRL program (R0A-2007-000-20032-0) and by the Korea Research Foundation (KRF-2005-205-C00010).

¹L. Thomas, M. Hayashi, X. Jiang, R. Moriya, C. Rettner, and S. S. P. Parkin, *Nature (London)* **443**, 197 (2006).

²D. A. Allwood, G. Xiong, M. D. Cooke, C. C. Faulkner, D. Atkinson, N.

Vernier, and R. P. Cowburn, *Science* **296**, 2003 (2002).

³J. Grollier, P. Boulenc, V. Cros, A. Hamzić, A. Vaurős, A. Fert, and G. Faini, *Appl. Phys. Lett.* **83**, 509 (2003).

⁴A. Yamaguchi, T. Ono, S. Nasu, K. Miyake, K. Mibu, and T. Shinjo, *Phys. Rev. Lett.* **92**, 077205 (2004).

⁵G. Meier, M. Bolte, R. Eiselt, B. Krüger, D.-H. Kim, and P. Fischer, *Phys. Rev. Lett.* **98**, 187202 (2007).

⁶M. Kläui, P.-O. Jubert, R. Allenspach, A. Bischof, J. A. C. Bland, G. Faini, U. Rudiger, C. A. F. Vaz, L. Vila, and C. Vouille, *Phys. Rev. Lett.* **95**, 026601 (2005).

⁷M. Hayashi, L. Thomas, C. Rettner, R. Moriya, X. Jiang, and S. S. P. Parkin, *Phys. Rev. Lett.* **97**, 207205 (2006).

⁸G. S. D. Beach, C. Nistor, C. Knutson, M. Tsoi, and J. L. Erskine, *Nat. Mater.* **4**, 741 (2005).

⁹S.-B. Choe and S.-C. Shin, *Appl. Phys. Lett.* **80**, 1791 (2002).

¹⁰S.-B. Choe and S.-C. Shin, *J. Appl. Phys.* **87**, 5076 (2000).

¹¹S.-B. Choe and S.-C. Shin, *J. Appl. Phys.* **81**, 5743 (1997).

¹²G. Tatara and H. Kohno, *Phys. Rev. Lett.* **92**, 086601 (2004).

¹³S.-B. Choe and S.-C. Shin, *Phys. Rev. B* **59**, 142 (1999).

¹⁴M. G. Pini and P. Politi, *J. Magn. Magn. Mater.* **313**, 273 (2007).